PREPRINT UCRL- 78062

CONF-760935--28

Lawrence Livermore Laboratory

Helium Generation and Diffusion in Graphite and Some Carbides

J. B. Holt, M. W. Guinan, D. W. Hosmer, R. H. Condit, R. J. Borg

September 17, 1976

This paper was prepared for submission to Technology of Controlled Nuclear Fusion, American Nuclear Society, Richland, Washington, Sept. 21-23, 1976.

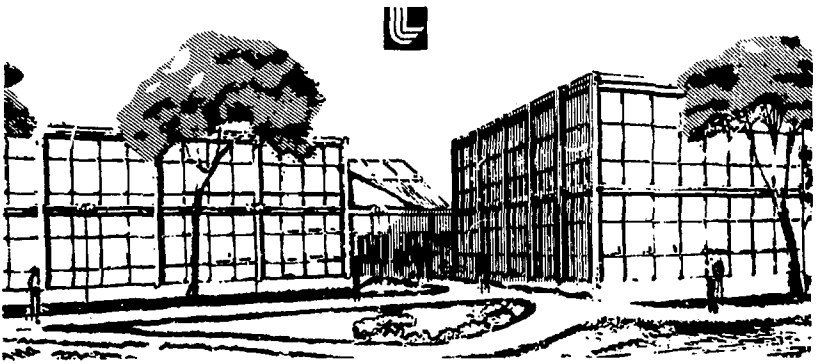

HELIUM GENERATION AND DIFFUSION IN GRAPHITE AND SOME CARBIDES

J. B. Holt, M. W. Guinan, D. W. Hosmer, R. H. Condit, and R. J. Borg

LAWRENCE LIVERMORE LABORATORY

The cross-section for the generation of helium in neutron irradiated carbon has been found to be 654 mb at 14.4 MeV and 744 mb at 14.9 MeV. Extrapolating to 14.1 MeV (the fusion reactor spectrum) gives 615 mb. The diffusion of helium in dense polycrystalline graphite and in pyrographite has been measured and found to be $D = 7.2 \times 10^{-7}\ m^2 s^{-1}$ exp (-80 kJ/RT). It is assumed that diffusion is primarily in the basal plane direction in crystals of the graphite. In polycrystalline graphite the path length is a factor of $\sqrt{2}$ longer than the measured distance due to the random orientation mismatch between successive grains. Isochronal anneals (measured helium release as the specimen is steadily heated) were run and maximum release rates were found at 200°C in polycrystalline graphite, 1000°C in pyrographite, 1350°C in boron carbide, and 1350° and 2400°C (two peaks) in silicon carbide. We conclude that in these candidates for curtain materials in fusion reactors the helium releases can probably occur without bubble formation in graphites, may occur in boron carbide, but will probably cause bubble formation in silicon carbide.

INTRODUCTION

In some conceptual designs of fusion reactors the use of graphite and other carbon containing materials has been proposed[1] as a curtain to protect the metallic first wall and reduce high Z impurity buildup in the plasma. Recent studies have examined this concept further.[2,3] Since these liners will be bombarded with high energy neutrons and charged particles, one may expect that their utility will be controlled by the particle - solid interactions. Our interests are directed to the problems which occur when 14 MeV neutrons generate helium within the solid by nuclear reactions.

Immediate questions which should be resolved are: (1) how much helium will be generated and (2) can the generated helium diffuse out from the curtain. The amount of helium produced is directly related to the total of n, α cross-sections, and although the cross-sections of the various α-producing reactions have been calculated, there is disagreement as to their correct values. So far as we are aware, the total cross-section for helium generation in carbon has never been verified by directly measuring the amount of helium generated within a solid sample.

With regard to helium migration one worries that phenomena similar to those noted in metals may occur; large concentrations of helium can have disastrous

effects on their mechanical properties, particularly at high temperature. Since helium diffusion in graphite has not been measured, the possible severity of this problem has been undetermined. Other carbon compounds have been considered also, and require detailed examination. This paper reports directly measured helium generation rates and diffusion in graphite and migration in two common carbides, boron carbide and silicon carbide.

MATERIALS

Structure might be expected to strongly influence the diffusion of helium in a solid. For this reason, two different types of graphite were selected for our experiments, dense polycrystalline graphite and pyrographite. The materials used were identical with those used in a previous diffusion study at this laboratory.[4] The polycrystalline graphite was ZTA brand manufactured by the National Carbon Company. It has a density of 2.11 g cm^{-3} with an average crystallite size of about 27 x 40 nm (i.e. L_a x L_c), and the proportion of disorder layers is small. Porosimetry measurements indicated that the maximum void size was 0.3 μm with 50% well below 0.1 μm. Chemical analysis revealed impurities to be Ca 50, Ti 40, and Si 10 ppm.

The pyrographite has a density of 2.20 g cm with subgrains having a diameter of about 15 nm. An X-ray determination of the relative orientation of the cone axes revealed the material to be highly oriented with a least 94% of the 001 poles lying within 5° of the mean axis. Impurities were found to be Ca 3, Al 20, and Si 10 ppm.

Silicon carbide, SiC, crystalline platelets had been prepared by the chemical vapor deposition process at 2650°C. They are clear but with a slight greenish cast and appear to have good crystal perfection. We have not analyzed them, but because of the high growth temperature they are believed to be pure aside from possible nitrogen and oxygen contamination.

Boron carbide, B_4C, was prepared by hot pressing high purity boron carbide powder to a density of 99% of theoretical. The grain size in the material is 10 μm. Impurities are Fe 150 ppm, Al 100 ppm, Be 25 ppm, Ca 20 ppm, Si 10 ppm, Mg 10 ppm.

SAMPLE PREPARATION AND IRRADIATION

Both the graphite and pyrographite were cut into rectangular slabs 10 mm x 10 mm and 0.15 to 0.25 mm thick. The pyrographite was cut with the c-direction (001 pole) normal to the large surface. The boron carbide sample was set of three irregular lumps weighing a total of 0.05 g with dimensions of roughly 2 mm on an edge. The silicon carbide plateletts with their c-axes normal to the large platelet area were 0.3 mm thick, and a 20 mm^2 area piece weighed 0.02 g.

The specimens were irradiated with approximately 14.8 MeV neutrons produced at the RTNS (Rotating Target Neutron Source) at the Lawrence Livermore Laboratory. The fluence varied from about 10^{16} to 10^{18} neutrons cm^{-2}. Details of the irradiation procedure are described elsewhere.[5]

After irradiation the helium content was determined by heating the specimen in vacuum and measuring the outgassing using a mass spectrometer of special design.[6] This equipment has been developed so as to be capable of easily measuring 10^{10} atoms of helium; since each sample contained from 10^{12} to 10^{13} atoms of helium, the experimental error was reduced to a minimum. One sample at a time was heated to the desired temperature by a tungsten mesh furnace. Thermocouples of Pt-Pt/Rh were attached to the heater. Both isochronal (controlled

heat rate with measurement of helium output at regular intervals) or isothermal anneals were carried out depending on the type of information desired.

HELIUM PRODUCTION CROSS-SECTION

Data primarily obtained for diffusion measurements was also processed to obtain cross-section values. During the irradiation the samples were stacked to minimize α-losses. Dosimetry foils, placed at each end of a stack of four to six samples, were used to determine fluences on individual samples by interpretation using the known dependence of neutron flux on position.[5,7]

After determination of the total helium content of each sample, corrections for α-losses were made taking into account the forward peaked α-spectrum. These were less than 0.5% for all but one sample for which the correction amounted to 4%. Loss from samples by room-temperature diffusion escape of the helium need not be taken into account, based upon extrapolation of our diffusion data to room temperature which suggests a possible loss of no more than 0.5% per year, and all samples were retained for less than this time, typically a few months.

Six of the nine samples were in a position where the average neutron energy was 14.9 MeV. The remaining three saw an average neutron energy of 14.4 MeV.

The total helium production cross-sections at each energy were determined using the $^{93}Nb(n,2n)^{92m}Nb$ cross-section which is taken as 467 mb at 14.4 MeV and 458 mb at 14.9 MeV[8] for determination of total neutron fluence.

The results are given below:

Neutron Energy	Cross-Sections for Helium Production
14.4 MeV	654 ± 92 mb
14.9 MeV	744 ± 60 mb

The weight fraction of samples in the two exposures was 0.2 and 0.8 in the lower and higher energies, respectively.

Helium is produced in carbon either one atom at a time through the reaction

$$^{12}C(n,\alpha_0)^{9}Be \qquad (1)$$

or three atoms at a time by reaction

$$^{12}C(n,n')3\alpha \qquad (2)$$

which includes the reactions

$$^{12}C(n,n')^{12*}C(\alpha)^{8}Be(2\alpha) \qquad (3)$$

and

$$^{12}C(n,\alpha)^{9*}Be(n')^{8}Be(2\alpha) \qquad (4)$$

as well as a possible four particle breakup. In order to compare with data available in the literature, we have subtracted the value of reaction (1) cross-section (75 ± 10 mb) from our results. This cross-section has been measured in this energy range by a number of investigators[9-16] and appears well defined. The measured values are shown in Fig. 1 as filled circles. Thus, we are left with values of 669 and 579 mb for the helium production from three-alpha processes. Dividing by three, we have 193 ± 31 mb at 14.4 MeV and 223 ± 20 mb at 14.9 MeV for the composite reaction process, equation (2), and these values are compared with literature values in Fig. 1.

Our values are shown as open circles with error bars based on deviations of individual samples from the mean. The open squares and triangles are the nuclear emulsion data of Green and Gibson[17] and Frye et al.[18], respectively. The filled triangles are the data of Frye et. al. corrected for missed three-pronged α-stars in their emulsions under the assumption that all events proceed through excited states of carbon-12 by reaction (3). The solid line represents more recent data on the expected sum of all contributions from

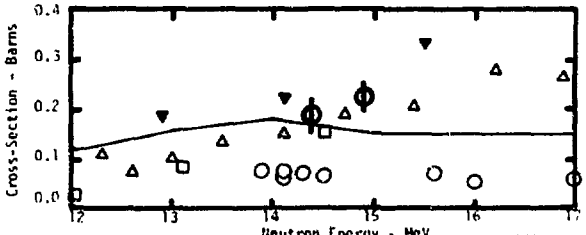

Fig. 1: Cross-Section Data: ⊕ our results, ○ n,α data[9-16], Green & Gibson[17], △ Frye[18], ▼ corrected Frye[18], the line is the sum of contributions from excited states of ^{12}C [16].

resolved excited states of carbon-12.[16]

Although the respective error bars overlap, the present data would indicate that Frye et. al. have overcorrected for missed stars. Support for this view is also found in Ref. 10. in which contributions from excited states of beryllium-9 were reported to be ~80 mb in this energy range. This discussion has taken no account of the possible reactions in carbon-13, but even assuming the n,α_1 cross-section to be zero would only introduce an error of 1.1%, the concentration of this isotope in the natural material. No evidence for a large cross-section has appeared, on the other hand, and therefore any contribution may be neglected.

The present results are in quite good agreement with existing nuclear data and are the result of a direct determination of helium production independent of any assumptions concerning the nuclear reactions involved. If our data points are extrapolated, see Fig. 1, down to 14.1 MeV, the energy characteristics of a fusion reactor output, the cross-section appears to be 180 mb for the n,3α reaction and the helium production cross-section is 3 x 180 + 75 = 615 mb.

We do not have good measurements for the helium production rates in our compound materials, but published data allow an estimate. In silicon carbide the only cross-section data for silicon is for the ^{28}Si isotope which constitutes about 92 of the natural material. The total (n,α_1) cross-section for ^{28}Si at 14.1 MeV is about 48 mb.[19] Neglecting the possible contributions from the other two isotopes, we find that the helium production cross-section is then at least about 44 mb. The total helium production cross-section for silicon carbide at 14.1 MeV is then at least 615 + 44 = 660 mb per SiC molecule.

In boron carbide the boron cross-section at 14.1 MeV for $^{11}B(n,\alpha_1)^8Li$ is 30 mb.[20] However, since the ^8Li shortly decays to 2α the helium production cross-section is 3 x 30 mb or 90 mb. The cross-section for the $^{10}B(n,2\alpha)^3H$ is 90 mb and for ^{10}B $(n,n'2\alpha)^2H$ is 110 mb[21] and the sum of these two, together with the factor for 2, makes the production cross-section 400 mb. The weighted average for boron taking the isotopic abundances into account gives a cross-section for helium production of 150 mb. Thus, in B_4C the cross-section becomes 4 x 150 + 615 mb = 1220 mb per molecule.

ISOCHRONAL ANNEALS

Preliminary isochronal measurements establish the temperature range for the subsequent isothermal runs from which diffusion coefficients may be derived. Samples typically contained 50-100 x 10^{-9} atom fraction of He. The results for ZTA graphite and pyrographite are shown in Fig. 2 which is a plot of the fractional release per unit time versus release temperature and clearly shows a difference between the two types of graphite. For the ZTA graphite the release rate drops to zero above 700°C while a temperature of nearly 1400°C is required to release all of the helium from the pyrographite. The diffusion analysis which follows shows that this is primarily due to the geometry of the samples.

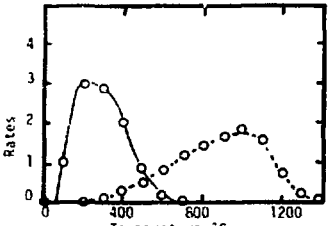

Fig. 2: Helium Reslease Rates- Solid is ZTA, Dashed is Pryographite Heated at 10 /min.

Isochronal measurements for boron carbide and silicon carbide are shown in Figs. 3 and 4. The helium atom concentrations were 23 x 10^{-9} per molecule of B_4C and 9 x 10^{-9} per molecule of SiC. The boron carbide melts at 2450°C, but almost the last portions of the helium had escaped before it reacted with the tungston heater at 2270°C. The silicon carbide on the other hand, still retained about 40% of its

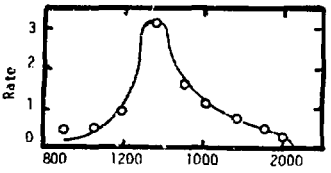

Fig. 3: Helium Release Rate From Boron Carbide. The heat rate was 10 C/min.

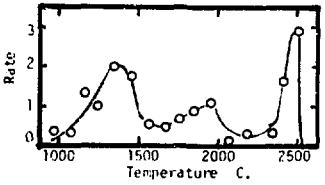

Fig. 4: Helium Release Rate from Silicon Carbide. The heat rate was 10 C/min.

helium at the time when it reactively melted into the tungsten at 2500°C. It also exhibited the first release peak in the region around 1350°C.

DIFFUSION ANNEALS

To determine the isothermal release rates, the samples were rapidly heated to a pre-selected temperature where the helium outgassing was measured as a function of time. Fig. 5 shows a typical fractional release curve. The initial helium concentration was assumed to be constant throughout the graphite slab, since it was produced uniformly by the irradiation and no loss while standing at room temperature was expected. However, given this initial boundary condition, the analyses for ZTA and pyrographite must differ. The pyrographite samples are highly oriented with basal plane being parallel with the long directions of the samples. Two kinetic equations might be considered in a description of the rate of helium release depending on the direction of diffusion.[4] For the two diffusion directions escape through the face vs. through the edge, the following equations would be appropriate:[22]

$$F^2 = \frac{16\,Dt}{h^2} \quad \text{(c-direction)} \qquad (5)$$

$$1 - (1 - F)^{1/2} = \frac{D}{d}\frac{t}{2} \quad \text{(a-direction)} \qquad (6)$$

where F is the fraction released, h is the thickness of the slab, d is the width of the slab, t is the time, and D is the diffusion coefficient. Although the pyrographite data fit both equations well, the linear correlation was maintained for longer fractional losses using equation (6). Typical plots are shown in Fig. 6. This is one reason for believing that helium diffuses preferentially in the a-direction and escapes at the edge which is consistent with previous diffusion measurements of other elements.[4]

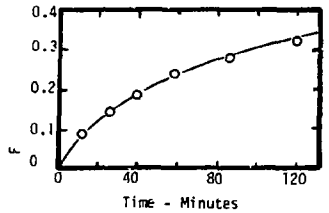

Fig. 5: Helium Release vs. Time Pyrographite 642°C. is Fraction Released.

In the case of the ZTA graphite, equation (5) has been used. Because of the random orientation of the grains, it is to be expected that the bulk of the release would be through the large faces. Note that the effective dimensions are different for ZTA and pyrographite; they are taken in the thin direction for the former and in the long dimension for the latter. Also, we have noted that the path length in the polycrystalline material is greater than the geometrical distance if one assumes basal plane diffusion only, because the crystallites are not aligned. The effective diffusion distance is greater in ZTA, although it has some crystallite preferred orientation as described in Ref. 4. We estimate that the coefficient normal to the flat surface of our ZTA specimens is less than along the basal plane direction by a factor of .48.

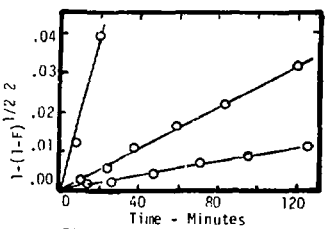

Fig. 6: Helium Release vs. Time - Pyrographite at 540, 642, and 845°C.

Therefore, to bring our ZTA data up to the pyrographite data we have simply multiplied by an approximate factor of 2. The diffusion coefficients derived in this way are plotted in Fig. 7.

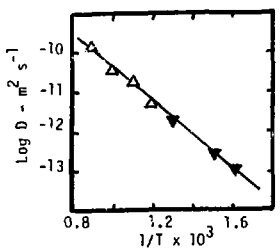

Fig. 7: Diffusion Coefficient vs. 1/T. Open Triangles ZTA, Closed Triangles Pyrographite.

The equality of the D values in both graphites demonstrates the mechanism to be the same. The required correction by the factor of 2 unequivocally demonstrates that diffusion occurs predominately along the basal plane and not parallel to <C>. However, we cannot distinguish between true interstial diffusion and sub-boundary diffusion. The values of D_o appear to be consistant with either mechanism and the geometrical correction would apply in either case. It is worth remembering that previous studies[4] have shown that diffusion of Ag, U, Th, Li, and Ra proceeds via the internal surfaces provided by sub-grains and not interstitially. The lack of interstitial diffusion in fact reflects the almost total lack of solubility of these elements in graphite. Whether or not this is also the case for helium will require further information.

DISCUSSION

The rates of helium generation in the materials studied here can be estimated for reactor operating conditions assuming a neutron flux of 10^{15} cm^{-2} s^{-1}, a value which might be expected near the plasma. The mole fractions after a year would be He/C = 1.9×10^{-2}, He/SiC = 2.1×10^{-2}, and He/B_4C = 3.9×10^{-2} if there were no escape of the helium. The possibility that this helium will be released concurrent with generation is clearly important.

Our finding that helium release from graphite, particularly if polycrystalline can be rapid in the temperature range proposed for a fusion reactor curtain, i.e. 1000 - 2300°C[1], is encouraging. It is supported by related work on ion implantation of 100 keV helium ions into graphite cloth[23] in which at 400 and 800°C no detectable surface damage was visible whereas equivalent irradiation at room temperature

produced considerable flaking. Thus, it appears that helium will not produce any direct damage effects in graphite. It remains to be seen whether or not it influences displacement damage mechanisms.

Our studies in the carbides may not provide a basis for complete evaluation at this time, because the influence of grain size has not been evaluated, and the slower escape of helium from silicon carbide than from boron carbide may be due merely to the large crystallite size. However, the appearance of two peaks in the silicon carbide is reminiscent of similar observations in copper[24] and steel[25], where bubble formation is proposed to explain the retention up to the melting point. This would be mostly a property of the bulk material and only partially dependent on grain size. Clearly, evaluation of the applicability of these carbides as curtain materials will require recognition of the probably role of helium generation and possible bubble formation.

ACKNOWLEDGEMENTS

We are indebted to Mr. William Parrish for some of the helium release measurements, Dr. Ralph M. Potter of the General Electric Company, Cleveland, Ohio, for supplying the silicon carbide, and Dr. W. Eatherly of the National Carbon Company for the donation of the ZTA graphite.

REFERENCES

1. G. L. Kulcinski, Radiation Effects and Tritium Technology for Fusion Reactors, J. S. Watson and F. W. Wiffen, Eds., National Technical Information Service, U. S. Dept. Commerce (1976), p. I-17.

2. H. I. Avci and G. L. Kulcinski, ibid. p. I-437.

3. W. J. Gray, W. C. Morgan, and G. L. Tingey, "Potential for Graphite Use Adjacent to the Plasma in Nuclear Fusion Reactors," BNWL-2078, Battelle Pacific Northwest Laboratories (1976).

4. J. R. Wolfe, D. R. McKenzie, R. J. Borg, J. Appl. Phys. 36 1906,3364 (1965).

5. R. A. VanKonynenburg, "Neutron Dosimetry for Foil Samples Irradiated with the LLL RTNS," UCRL-51393, Rev. 1 (1974).

6. R. W. Crawford, J. W. Frazer, and J. B. Holt, Rev. Sci. Instr. 42: p. 674 (1971).

7. J. O. Seagrave, "D(d,n)He^3 and T(d,n)He^4 Neutron Source Handbook," LAMS-2162, (1958)

8. D. Nethaway (Private Communication).

9. E. R. Graves and R. W. Davis, Phys. Rev. 97 p. 1205 (1954).

10. R. A. Al-Kital and R. A. Peck, Jr., Phys. Rev. 130 p. 1500 (1963).

11. M. L. Chatterjee and B. Sen, Nucl. Phys. 51 p. 58, (1964).

12. M. Brendle et. al., J. Inorg. Nuc. Chem. 30 p. 1 (1968).

13. D. Kopsch and S. Cierjacks, Nucl. Instr. Methods 54 p. 277 (1969).

14. H. Kitazawa and N. Yamamuro, J. Phys. Soc. Japan 26, p. 600 (1969).

15. S. Kardonsky, H. L. Finston and E. T. Williams, Phys. Rev. C 4, p. 840 (1971).

16. R. J. Howerton et. al., "An Integrated System for the Production of Neutronics and Photonics Calculational Constants," Volume 15 Part B (ENDL) UCRL-50400 (1976).

17. L. L. Green and W. M. Gibson, Proc. Phys. Soc. (London) A62, p. 296 (1949).

18. G. M. Frye, L. Rosen and L. Stewart, Phys. Rev. 99, p. 1375 (1955).

19. L. Colli, I. Iori, M. G. Marcazzan, and M. Milazzo, Nucl. Phys. 43, p. 529 (1963).

20. A. H. Armstrong and G. M. Frye, Jr., Phys. Rev. 103, p. 335 (1956).

21. G. M. Frye, Jr. and J. H. Gammel, Phys. Rev. 103, p. 328 (1956).

22. W. E. Garner (Editor), Chemistry of the Solid State, Butterworths.

23. R. Elkern, S. K. Das, and M. Kaminsky, in CTR Quarterly Progress Report, Oct.-Dec., 1975, ANL/CTR-75-5, Argonne National Laboratory (1976).

24. J. R. Cost, R. G. Hickman, J. B. Holt, and R. J. Borg, see Ref. 1, p. II-234.

25. J. B. Holt, D. W. Hosmer, and R. A. Van Konynenburg, see Ref. 1, p. II-280.

Work performed under the auspices of the U.S. Energy Research & Development Administration under contract No. W-7405-Eng-48.